Hindawi
Journal of Nanomaterials
Volume 2022, Article ID 2042754, 11 pages
https://doi.org/10.1155/2022/2042754

Research Article

Exosomes Derived from Gold Nanorod Engineered Vascular Endothelial Cells Inhibit Tumor Growth via Disrupting the TGFβ Pathway

Weiye Zhu,[1] Rui Zhang,[1] Zichang Zhao,[1] Na Zhao,[1] Xiao Gui,[1] Xiao Cui,[1] Ni Shen,[1] Jiawei Zhao,[1] Guangping Gao,[1] Haorui Zhang,[1] Chenyang Huan,[1] Yukun Zhou,[1] Yanjie Li,[1] Jianhua Zhang,[1] Hongyuan Song,[1,2] and Wei Shen[1]

[1]*Department of Ophthalmology, Shanghai Changhai Hospital, Naval Medical University, Shanghai 200433, China*
[2]*Department of Ophthalmology, Shanghai General Hospital, Shanghai Jiao Tong University School of Medicine, Shanghai 200080, China*

Correspondence should be addressed to Jianhua Zhang; drzhangjianhua@163.com, Hongyuan Song; hongyuansong@hotmail.com, and Wei Shen; shenwzz@163.com

Received 17 August 2021; Revised 2 February 2022; Accepted 28 February 2022; Published 24 March 2022

Academic Editor: Mohammad Owais

Exosomes are nanosized extracellular vesicles which are emerging as novel therapeutic nanoparticles. This paper reports a novel concept of engineering exosomes using nanomaterial inside the vascular endothelial cells (ECs). Gold nanorods (GNRs) could inhibit EC division and internalized GNRs located in endosomes of binucleated ECs. The GNRs could alter the composition of bioactive molecules loaded in exosomes. The engineered EC-derived exosomes could inhibit tumor cell proliferation, migration, and invasion in vitro and suppress tumor growth in vivo. miRNA sequencing showed that the engineered exosomes contained various miRNAs that could disrupt the TGFβ pathway. Further data suggested that the engineered exosomes could suppress the expression of TGFβ1 and TGFβ2, thus inhibiting the activation of SMAD2 and SMAD3. These data highlighted the therapeutic potential of engineering exosomes using nanomaterials.

1. Introduction

Tumor is one of the leading causes of mortality over the past decades [1]. The therapeutic efficiency of surgery, chemotherapy, radiotherapy, and immunotherapy is far from satisfactory; thus, novel therapeutic methods and agents need further investigation [1, 2]. These issues are where the rapidly developed nanotechnology comes into address. Due to their unique physicochemical properties, nanomaterials have widely been used for bioimaging, diagnosis, drug delivery, and tumor therapy [3]. These progresses in research have been translated to new drug applications which are further evaluated by the US Food and Drug Administration (FDA) [4]. Recently, Zanganeh et al. find that adenocarcinoma cells coincubated with iron oxide nanoparticles (ferumoxytol) and macrophages show increased caspase-3 activity [5]. In a transwell coculture system, there is no direct contact between two different cells; thus, the secreted molecules play a major role in tumor cell apoptosis induction. This work inspires the idea that cells treated with nanomaterials might be able to secret therapeutic bioactive molecules for medical applications. Recent studies reveal that iron oxide nanoparticles could engineer mesenchymal stem cells to produce bioactive exosomes, which present promising therapeutic application in ischemic stroke and heart infarction [6–7].

Exosomes are naturally derived nanoparticles that ranged from 40 nm to 150 nm containing abundant bioactive molecules, such as proteins, lipids, and RNAs, which mediate intercellular communication of different cell types in the body [8]. Unlike other extracellular vesicles, exosomes do not originate from the direct budding of the plasma

membrane but derived from multivesicular bodies (MVBs). The MVBs belong to a subset of endosomes which contain membrane-bound intraluminal vesicles (ILVs) [9]. The majority of MVBs will fuse with lysosomes leading to the degradation of bioactive content. Others fuse with cell membrane to release ILVs which are known as extracellular exosomes [9]. Exosomes secreted by many cells have been reported to play vital roles in the occurrence and progression of tumor [10]. The engineering of exosomes has been achieved by loading therapeutic RNA and decorating exosomes with multiple molecules, which have been proved to disrupt the growth of tumor [11]. However, engineering of exosomes inside their mother cells are barely investigated. Previous studies show that exosomes purified from bronchoalveolar lavage fluid of iron oxide nanoparticle-treated mice could activate the immune system [12, 13]. Gold nanoparticles internalized by cells could be released using exosomes as shuttles, and the gold nanoparticle containing exosomes could be used for miRNA delivery with higher efficiency [14, 15]. These investigations pave a possible road that nanomaterials could engineer exosomes inside the mother cell for therapeutic usage.

In this study, we showed that PSS-GNRs could inhibit the cytokinesis of vascular endothelial cells and then alter the bioactive molecules in the secreted exosomes. The engineered exosomes contain various miRNAs that target the TGFβ pathway and were able to suppress tumor growth *in vitro* and *in vivo* via disrupting the TGFβ pathway (Scheme 1). This work highlights the potential of engineering exosomes inside ECs using nanomaterials.

2. Experimental

2.1. Synthesis of Gold Nanorods. Gold nanorods (GNRs) were prepared as we described previously [16]. After being washed once with pure water, GNRs were dispersed in polysodium-p-styrenesulfonate (PSS) aqueous solution (2 mg/mL PSS, containing 30 mg/mL NaCl). The reaction was stopped by centrifuge after incubation with PSS for 8 h at room temperature. After being washed twice, PSS-GNRs were dispersed in water for further usage. The characteristics of GNRs were assessed using a transmission electron microscope (TEM, H-7650, Hitachi, Japan), Fourier transform infrared spectra (FT-IR) (Perkin-Elmer Spectrum GX, USA) Zetasizer Nano ZS90, and BioTek synergy2 (BioTek, VT, USA).

2.2. Cell Lines. Human retinal endothelial cells (HRECs) were ordered from ScienCell (San Diego, USA) and cultured in complete endothelial cell medium.C918 cells were ordered from KeyGEN BioTECH (Nanjing, China), and were cultured in Dulbecco's Modified Eagle Medium (DMEM) supplemented with FBS (10%), L-glutamine (1%), penicillin (100 U/mL), and streptomycin (100 μg/mL). These cells were incubated at 37°C in a humidified atmosphere with 5% CO_2.

2.3. Observation of Binucleated HRECs. The F-actin cytoskeleton was stained with phalloidin. Briefly, cover glasses were used for the seeding of cells, and after being incubated with 40 μg/mL PSS-GNRs for 48 hours, the cover glasses were washed with phosphate-buffered saline (PBS). Then, the cells were fixed with 4% paraformaldehyde for 20 minutes. For better staining, 0.1% Triton X-100 was used to permeabilize the cell for 20 min at RT. After being washed twice, the cells were further stained with phalloidin and DAPI. Finally, an IX81 microscope was used to capture the fluorescent images.

2.4. Exosome Isolation. HRECs were cultured in 10 cm dishes, and when they grew to 30% confluence, they were treated with PSS-GNRs for 48 hours to collect the GNRs-Exo. HRECs without PSS-GNR treatment was set as the control group to collect the Con-Exo. Exosome-free medium was added into the dishes, and HRECs were cultured for another 48 hours. The culture medium was collected and used for exosome isolation. Ultracentrifuge was performed according to the following step: conditional medium was centrifuged at $300 \times g$ for 10 min; then, the supernatant was collected and centrifuged at $2000 \times g$ for 10 min, followed with centrifugation at $12000 \times g$ for 45 min. The supernatant was then ultracentrifuged (HITACHI, Japan) at $100000 \times g$ for 70 min. The pellets were washed with PBS and centrifuged at $100000 \times g$ for another 70 min. The pellets were resuspended with PBS and assessed with TEM and ZetaView (Particle Metrix, Germany).

2.5. Cellular Uptake Assay. The fluorescent dye Dil (10 μM, Beyotime, Shanghai, China) was added to GNR-Exo suspensions and then was incubated with exosomes for 20 min at RT. The stained exosomes were washed twice with PBS by ultracentrifugation at $100000 \times g$ for 70 min, and then were resuspended in PBS. C918 cells were incubated with Dil-labelled GNRs-Exo for 2 hours. Then, PBS was used to wash the C918 cells twice and 4% paraformaldehyde was used to fix the cells for 20 minutes. After rinsing twice with PBS, the cells were incubated with α-tubulin and DAPI for 30 min. Finally, a Zeiss LSM-710 confocal microscope was used to analyze the sample.

2.6. Cell Proliferation Assay. Cell Counting Kit-8 was used for the determination of cell proliferation with a 96-well plate. For HREC experiment, 2×10^3 HRECs were seeded into plates and were treated with PSS-GNRs for 48 hours. The supernatant was discarded and PBS was used to wash the cells twice. 110 μL fresh medium containing 10 μL CCK-8 was added into each well of the plate. After 2 hours, BioTek Synergy 2 was used to measure the optical density.

In the following cellular function assays, C918 cells without treatment were set as control. Thus, two groups of C918 cells were set: control and GNR-Exo treatment. For the C918 cell experiment, 2×10^3 cells were seeded into plates and were treated with GNRs-Exo for 48 hours. The supernatant was discarded, and PBS was used to wash the cells twice. 110 μL fresh medium containing 10 μL CCK-8 was added into each well of the plate. After 2 hours, BioTek Synergy 2 was used to measure the optical density.

2.7. Cell Migration and Invasion Assay. Transwell units with 8 μm pore size polycarbonate filter were used for cell migration assay. 2×10^4 C918 cells treated with GNRs-Exo for

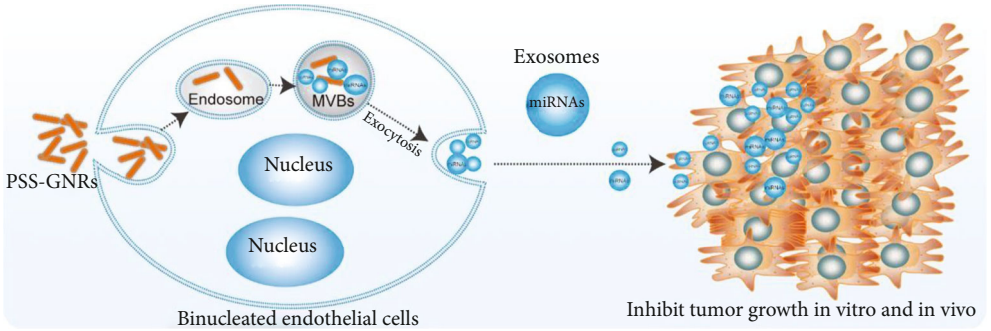

Scheme 1: Schematic illustration of engineering exosomes and their antitumor effect.

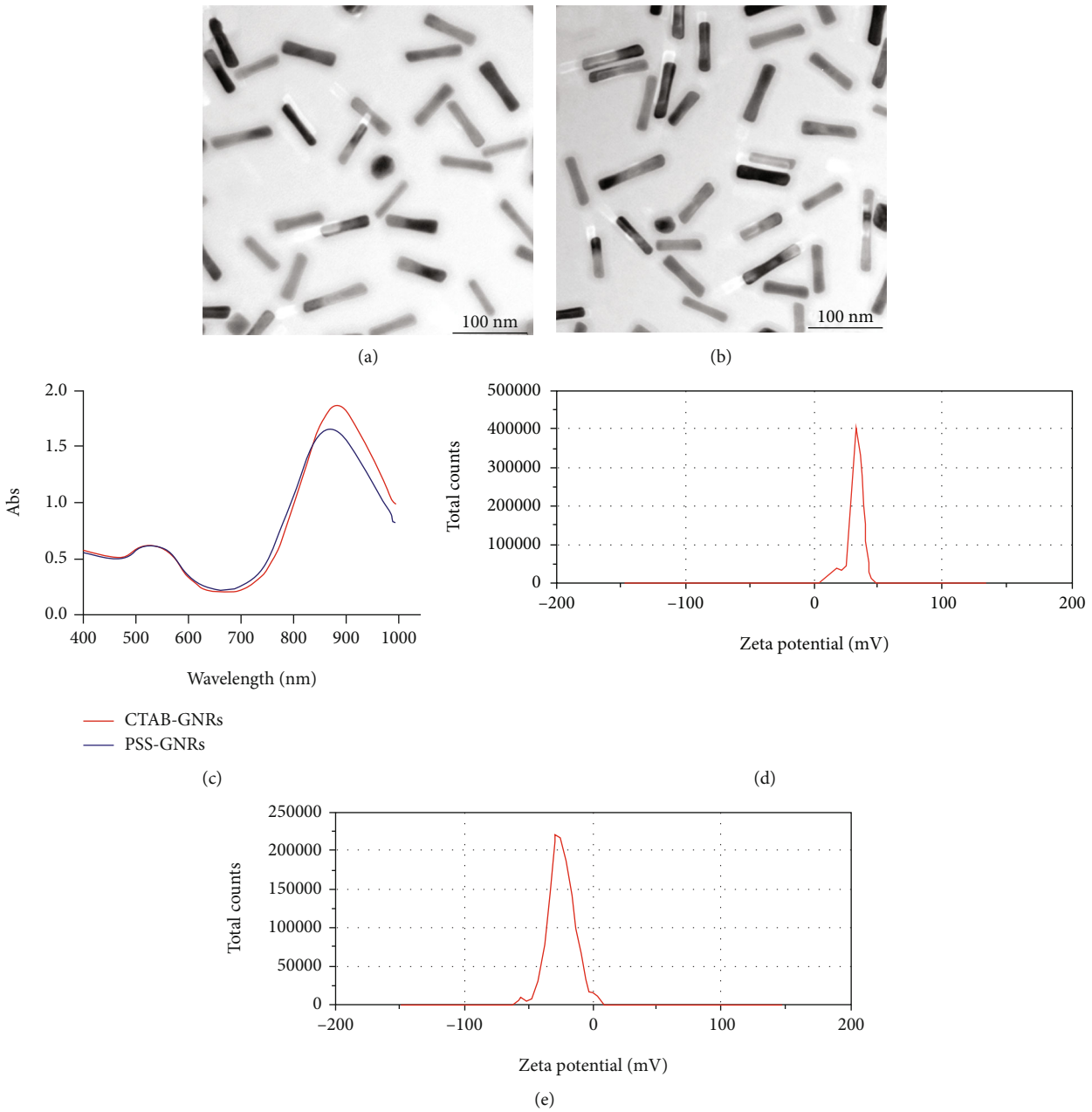

Figure 1: Characterization of GNRs: (a) TEM image of CTAB-GNRs; (b) TEM image of PSS-GNRs; (c) UV-vis absorption spectra of CTAB-GNRs and PSS-GNRs; (d) zeta potential of CTAB-GNRs; (e) zeta potential of PSS-GNRs.

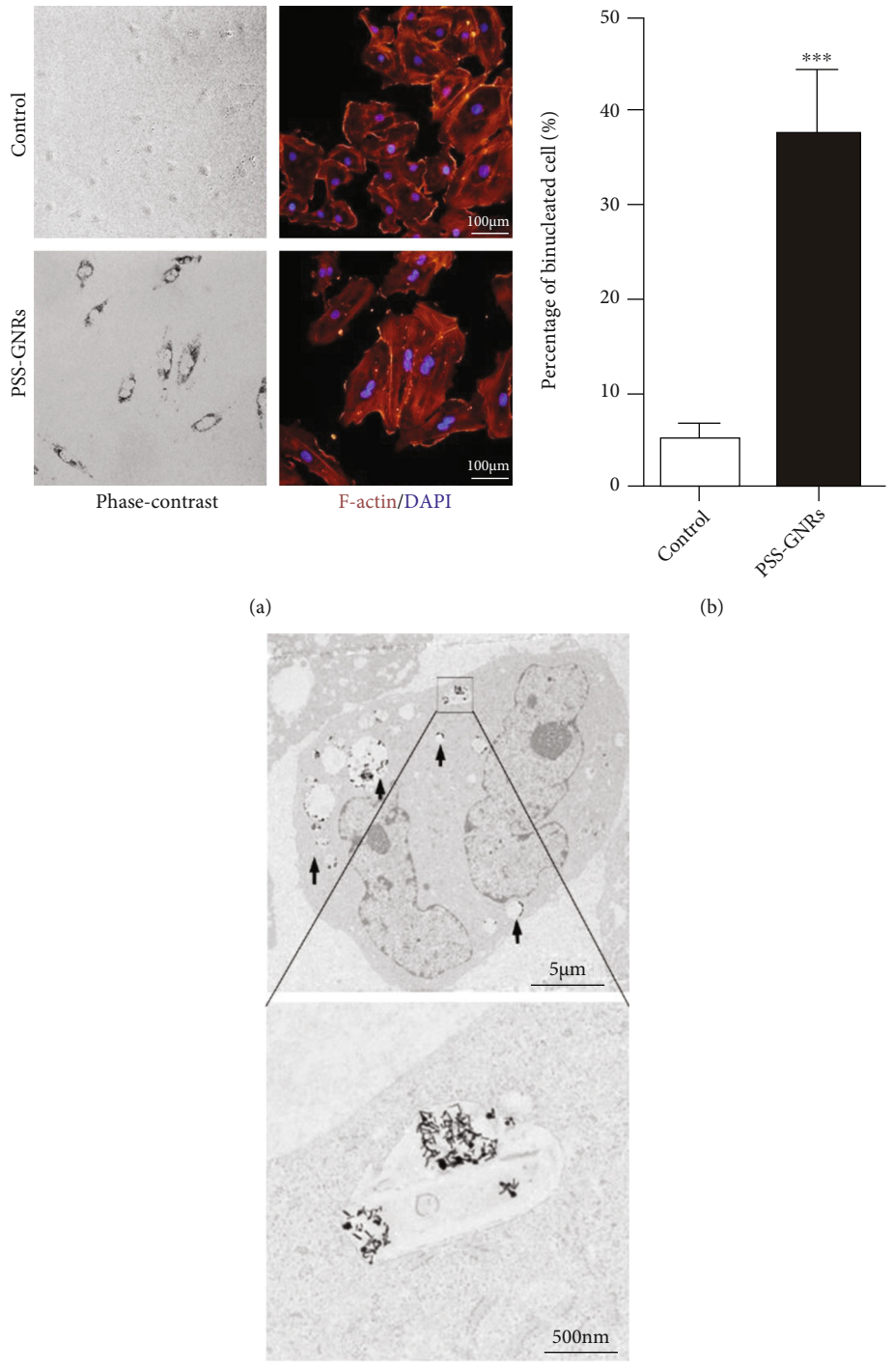

Figure 2: PSS-GNRs induce the binucleation of endothelial cells. (a) PSS-GNRs induce binucleation of ECs. Cells are stained with F-actin (red) and DAPI (blue) (scale bar 100 μm). The phase contrast images and immunofluorescent images were taken in the same field. (b) Quantitative analysis of binucleated cells in the control group and PSS-GNR-treated group. Data are presented as the means ± SD, $n = 4$ ($^{***}p < 0.001$). (c) TEM images of binucleated ECs treated with PSS-GNRs and the localization of PSS-GNRs. PSS-GNRs are mainly located in the endosomes of ECs as indicated by black arrows.

48 h in 0.5% FBS medium were seeded into the upper chamber of transwell. 800 μL DMEM containing 1% FBS and 30 μg/mL GNRs-Exo was added into the lower chamber. The cells were allowed to migrate for 12 hours, and then, 4% paraformaldehyde was used to fix the filters for 20 minutes. For cell invasion assay, Matrigel was used to coat the transwell units initially. Then, 2×10^4 C918 cells treated with GNRs-Exo for 48 h in 0.5% FBS medium were seeded

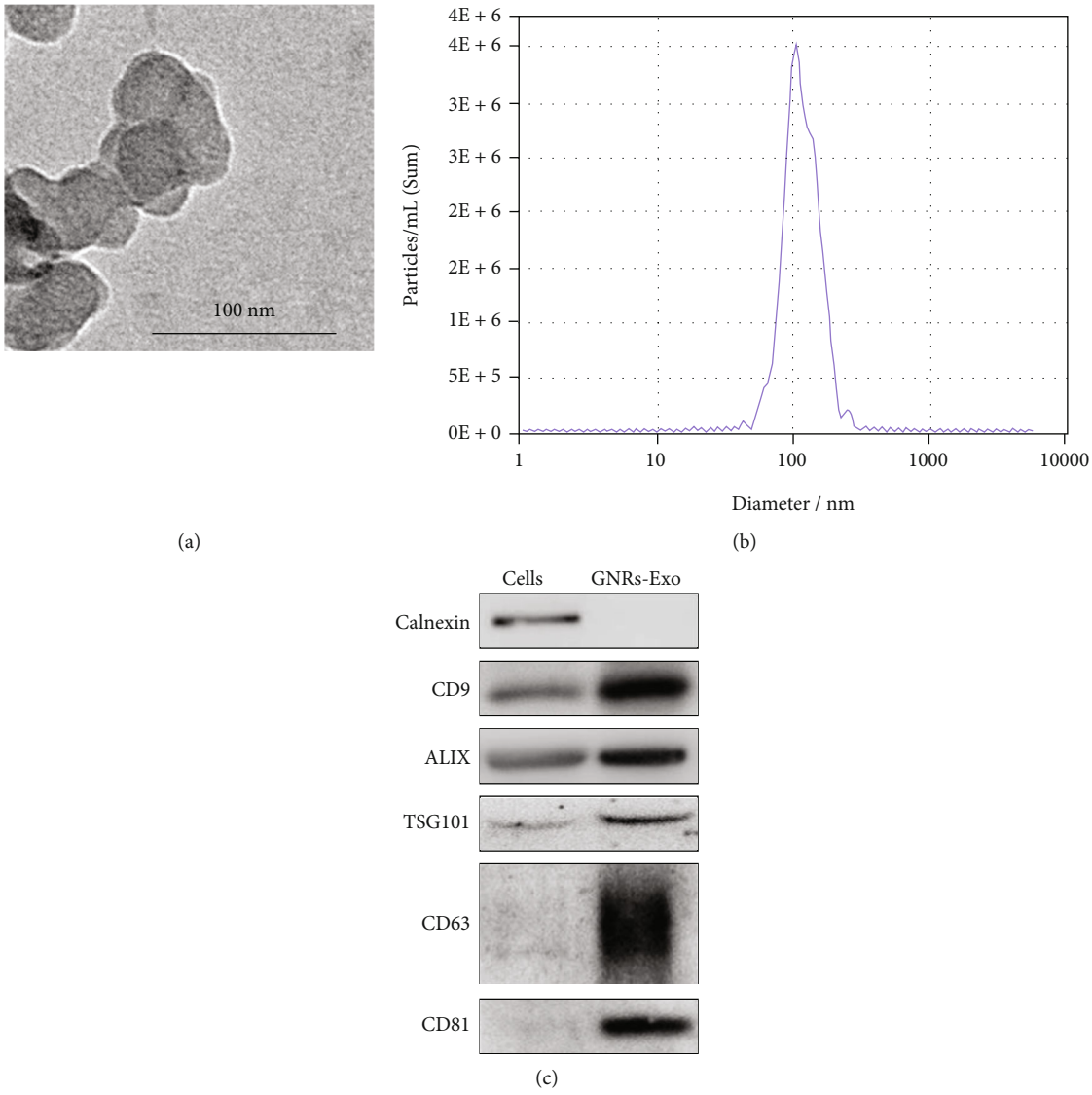

Figure 3: Characterization of exosomes. (a) Representative TEM image of exosomes (scale bar 100 nm). (b) Representative result of NTA shows the size distribution of exosomes. (c) Western blots confirm the presence of exosomal marker proteins CD9, ALIX, TSG101, CD63, and CD81 and the absence of exosomal negative protein calnexin.

into the upper chamber of transwell units. 800 μL DMEM containing 1% FBS and 30 μg/mL GNRs-Exo was added into the lower chamber. The cells were allowed to invade for 18 hours, and then, 4% paraformaldehyde was used to fix the filters for 20 minutes. Then, for the two experiments, a cotton swab was used to remove cells from the upper surface of the filter. Furthermore, 0.1% crystal violet was used to stain the filters for 15 minutes. IX81 microscope system was used to analyze the number of cells on the lower surface of the filter.

2.8. Xenograft Model. Male BALB/c nude mice (20-25 g) were purchased from the SIPPR-BK Experimental Animal Co., Shanghai, China. Animals were housed in polypropylene cages and animal manipulations were performed in accordance with the guidelines of the Animal Care and Use Committee of the Naval Medical University. A total of 8×10^6 melanoma cells in 100 μL PBS mixed with 100 μL Matrigel were subcutaneously injected into nude mice. Two weeks later, GNRs-Exo or Con-Exo were injected into the melanoma tumor twice a week for three weeks. Meanwhile, the size of xenograft was monitored every 4 days. The volume of xenograft was calculated using the following formula: volume = $a \times b^2/2$ (a represents length, and b represents width). The xenografts were finally extracted and weighed.

2.9. miRNA Sequencing. Total RNA was extracted from GNRs-Exo and Con-Exo using Trizol LS. The total RNA was sent to the Beijing Genomics Institute (Beijing, China) for further analysis. Fold change filtering (2-folds) was used to identify the differentially expressed genes. The MultiExperiment Viewer was used for hierarchical clustering with

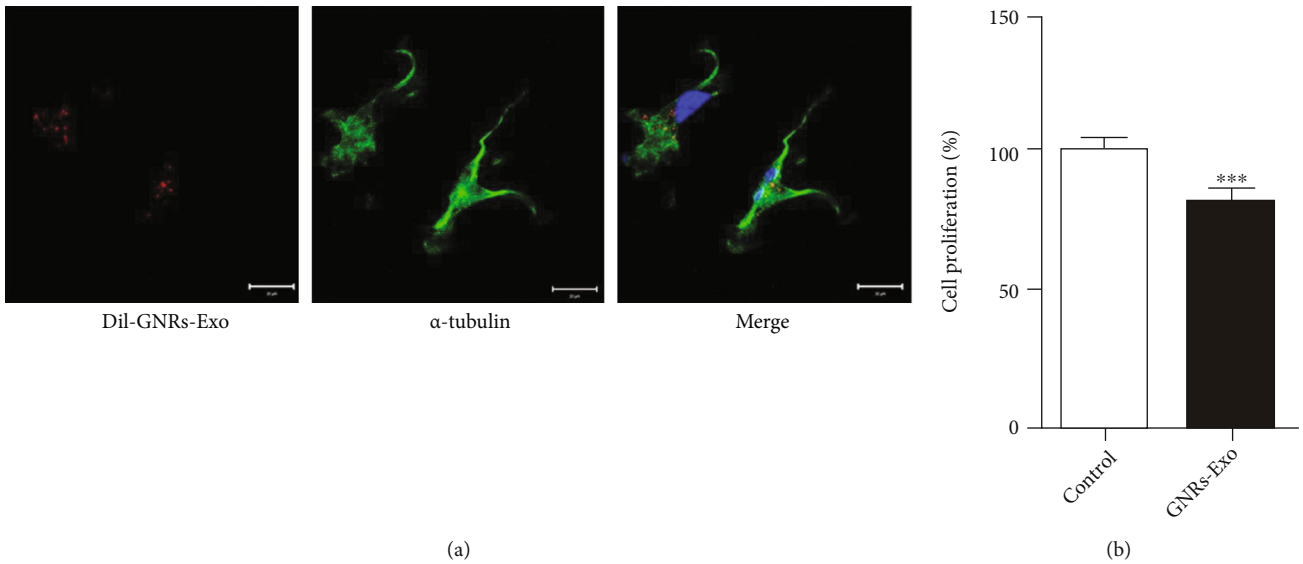

Figure 4: Internalization of exosomes by C918 cells. (a) Dil-stained GNRs-Exo are taken up by C918 cells. Dil-stained GNRs-Exo are shown in red; cells are stained with α-tubulin (green) and DAPI (blue) (scale bar 20 μm). (b) Quantitative analysis of cell proliferation in the control group and GNR-Exo-treated group. Data are presented as the means ± SD, $n = 5$ ($^{***}p < 0.001$).

average linkage. The KEGG pathway analysis was performed using the standard enrichment computation method.

2.10. Quantitative RT-PCR Analysis. Total RNAs from GNRs-Exo and Con-Exo were extracted using Trizol LS. The concentration and purity of RNA were assessed using Agilent 2100 (Agilent Technologies, USA). The RNA samples were used when the ratio of A260/280 and A260/A230 was larger than 1.8. Approximately 20-25 ng RNAs were transcribed to cDNAs using Mir-X miRNA qRT-PCR SYBR® Kit. Then, equal quantities of cDNA were used for real-time PCR with the control of U6. Reactions were incubated at 95°C for 30 s, followed by 45 cycles at 95°C for 10 s and 60°C for 30 s. For the dissociation curve step, the reactions were incubated at 95°C for 60 s, 55°C for 30 s, and 95°C for 30 s. The results were expressed as the mean relative value compared with control samples.

2.11. Western Blot Analysis. Modified lysis buffer with proteinase inhibitor cocktail was used to extract protein from exosomes and cells. 15 μg proteins were electrophoresed using SDS/PAGE gels (10%) and transferred to 0.22 μm polyvinylidene fluoride (PVDF) membranes. Nonfat milk (5%) was used to block the nonspecific sites for 2 hours. Then, indicated primary antibodies were used to incubate the membranes at 4°C overnight. Horse radish peroxidase-conjugated antibodies were further used to incubate the blot for 2 hours at RT. The blots were incubated with SuperSignal West Pico Chemiluminescent Substrate and visualized using the GeneGnome HR Image Capture System.

2.12. Statistical Analysis. All data were expressed as means ± standard deviation (SD) when the data were normally distributed. If the data were abnormally distributed, they were presented as medians (quartiles). One-way ANOVA was used to compare quantitative data, and SNK tests were further used for multiple comparisons. Statistical analysis was performed using GraphPad Prism8.0, and the data were considered statistically significant when $p < 0.05$.

3. Results and Discussion

GNRs synthesized using cetyltrimethylammonium bromide (CTAB) are toxic as CTAB is able to cause dysfunction of mitochondria [17]. Polyethylene glycol (PEG) is widely used to avoid toxicity of CTAB-GNRs, but there are reports showing that PEG can induce inflammation [18]. Polysodium-p-styrene sulfonate (PSS) has been reported to reduce toxicity of CTAB-GNRs significantly [19]. In the current study, we synthesized CTAB-GNRs as we previously reported and decorated them with PSS. The successful PSS coating was analyzed using FT-IR, which showed a remarkable band at 1215 cm^{-1}, 1176 cm^{-1}, and 1124 cm^{-1} (Fig. S1). The synthesized PSS-GNRs were uniform with the length of 77.5 + 6.5 nm and with the width of 15.5 + 1.1 nm (Figures 1(a) and 1(b)). Meanwhile, the decoration of PSS had no apparent effect on the morphology and longitudinal local surface plasmon resonance of GNRs but changed their zeta potential (Figures 1(c)–1(e)). PSS-GNRs could inhibit human retinal endothelial cell (HREC) proliferation dose dependently and a concentration of 40 μg/mL was chosen for subsequent experiments (Fig. S2).

In previous work, we found that GNRs were able to inhibit vascular endothelial cell cytokinesis thus disrupting angiogenesis [20]. Here, our data indicated that PSS-GNRs could also induce the formation of binucleated ECs and PSS-GNRs located in endosomes of ECs. The results showed that HRECs internalized PSS-GNRs abundantly, which appeared as black dots around cell nuclei under a phase contrast microscope (Figure 2(a)). Then, the cells were stained with F-actin and DAPI, which showed a high ratio of binucleated HEECs in the PSS-GNR-treated group (Figure 2(a)).

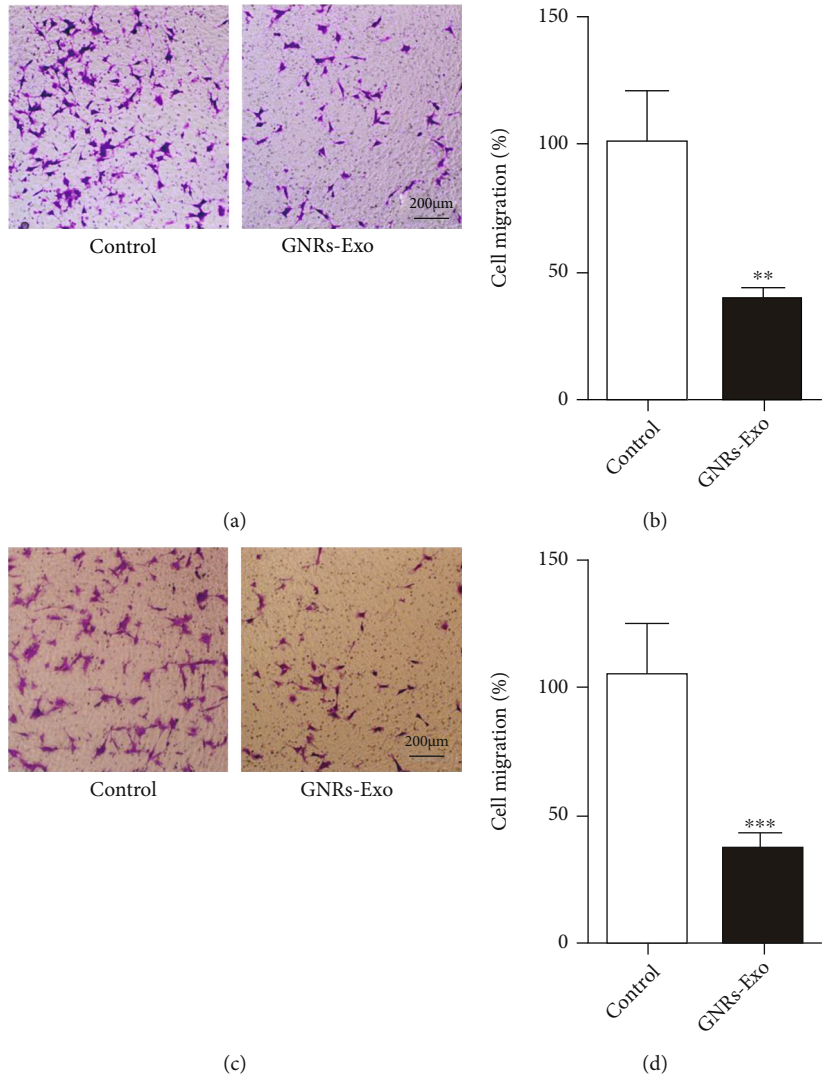

Figure 5: GNRs-Exo suppress tumor growth *in vitro*. (a) Representative images of cell migration. (b) Quantitative analysis of cell migration in the control group and GNRs-Exo-treated group. Data are presented as the means ± SD, $n = 4$ ($^{**}p < 0.01$). (c) Representative images of cell invasion. (d) Quantitative analysis of cell invasion in the control group and GNR-Exo-treated group. Data are presented as the means ± SD, $n = 4$ ($^{***}p < 0.001$).

The ratio of binucleated cells rose from 5% to 37% after the treatment of PSS-GNRs (Figure 2(b)). Binucleation of many cells is usually the terminally differentiated state. These cells no longer proliferate, and bioactive molecules secreted by the cells may be different from mononucleated cells [21]. GNRs with different decorations are internalized by cells through multiple pathways including clathrin-dependent and lipid raft-dependent pathway, which are then trafficked to endosomes [22, 23]. Consistent with these results, our data showed that the internalized PSS-GNRs are mainly located in the endosomes of HRECs (Figure 2(c)). Endosomes are the upstream organelle of exosomes and are the place where exosomes formed. The location of PSS-GNRs and the formation of binucleated cells suggested that exosomes secreted by these cells were reengineered compared with the exosomes derived from normal cells.

To better understand the properties of the exosomes, we performed subsequent experiments. The characteristics of PSS-GNR engineered exosomes (GNRs-Exo) were examined using a transmission electronic microscope (TEM), nanoparticle track analysis (NTA), and western blot. The GNRs-Exo presented typical "cup-shaped" morphology under TEM with the size of ~100 nm (Figure 3(a)). The average size of exosomes was 107.7 ± 2.0 nm observed using NTA, which was larger than that of TEM (Figure 3(b)). Exosomal markers CD81, CD63, CD9, TSG101, and ALIX were detected in GNRs-Exo, while calnexin was barely detected (Figure 3(c)). Calnexin is an integral protein of the endoplasmic reticulum (ER) which is reported negative in exosomes [24]. These data indicated that the separated GNRs-Exo were of high purity.

The angiogenic and oncogenic exosomes derived from endothelial cells, stem cells, and tumor cells have been investigated extensively [25, 26]. However, the studies of antiangiogenic and tumor suppressive exosomes are rarely reported. To further assess the effect of GNRs-Exo on tumor

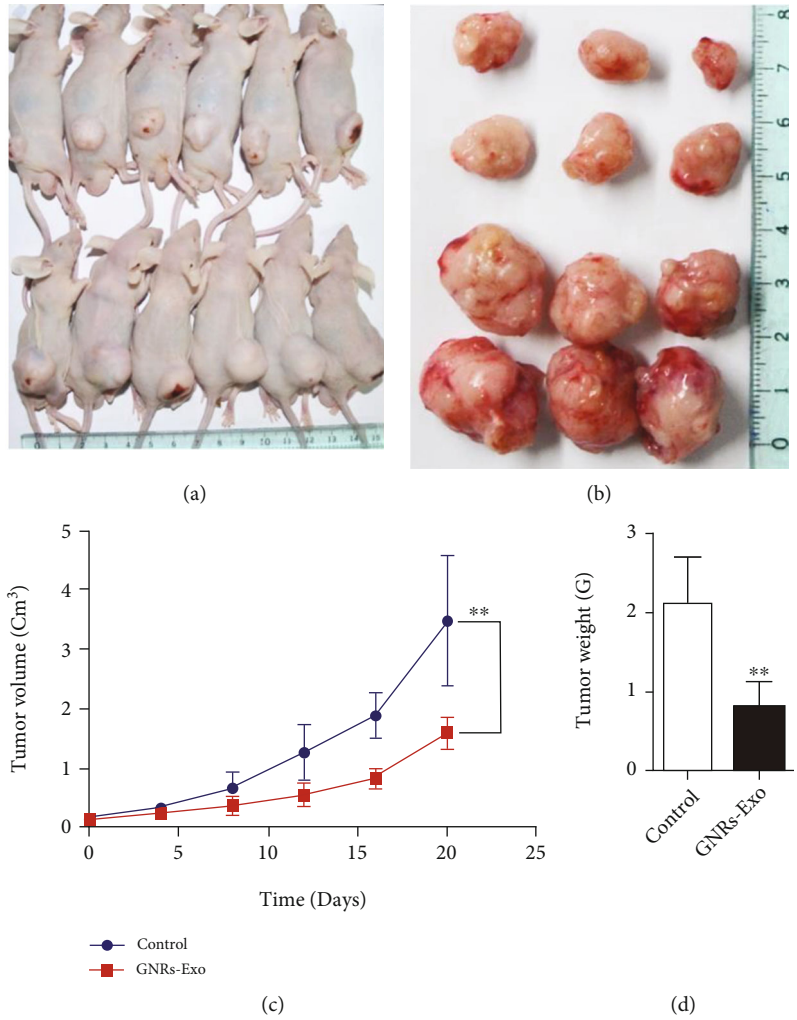

Figure 6: GNRs-Exo suppress tumor growth *in vivo*. (a) Representative photographs of mice in the control group and GNR-Exo-treated group. (b) Representative photographs of tumors in the control group and GNR-Exo-treated group. (c) Tumor growth curves for the control group and GNR-Exo-treated group. Data are presented as the means ± SD, $n = 6$ ($^{**}p < 0.01$). (d) Quantitative analysis of tumor weight in the control group and GNR-Exo-treated group. Data are presented as the means ± SD, $n = 6$ ($^{***}p < 0.001$).

cells, we initially examined whether GNRs-Exo could be taken up by tumor cells. As shown in Figure 4(a), Dil-stained GNRs-Exo were internalized and located around the nuclei of C918 (human choroidal melanoma cell) after incubating with C918 for 2 hours. One of the hallmarks of tumor is the uncontrolled growth of cells [27]. Our data showed that after culturing for 48 hours, GNRs-Exo could impair the proliferative ability of tumor cell by 19% (Figure 4(b)).

The metastasis of tumor cells to a distant part of the body is usually called stage IV tumor, which carries a very poor prognosis [27]. The tumor cells need to break down the barriers of extracellular matrix; therefore, the ability of migration and invasion of tumor cells is the key for metastasis [27]. Thus, we performed transwell assays to study the effects of GNRs-Exo on cell migration and invasion. Choroidal melanoma cells (C918) were pretreated with GNRs-Exo for 48 hours, and then, they were digested and seeded on the upper side of naked or Matrigel-coated transwell membrane for migration or invasion assay. The data indicated that GNRs-Exo could inhibit the migration of C918 by 60% (Figures 5(a) and 5(b)) and suppress the invasion of C918 by 65% separately (Figures 5(c) and 5(d)). Furthermore, a xenograft model was used to evaluate the effect of GNRs-Exo on tumor growth *in vivo*. The result showed that GNRs-Exo was able to reduce tumor growth significantly (Figures 6(a) and 6(b)). Tumors treated with GNRs-Exo grew slower as the mean volume reduced about 55% (Figure 6(c)) and the mean weight reduced about 62% (Figure 6(d)). All these data suggested that GNRs-Exo exhibit good antitumor effects both *in vivo* and *in vitro*.

A variety of bioactive molecules have been found in exosomes, including proteins, lipids, DNAs, mRNAs, miRNAs, and lncRNAs [8]. Among them, exosomal miRNAs have been studied extensively and have shown great potential in therapeutics. Mature miRNAs are 17-24 nucleotides (nt) long, single-stranded RNA molecules, which could regulate posttranscriptional gene expression. They involve in many biological processes including cell growth, cell migration, inflammation, and differentiation [28]. To better understand

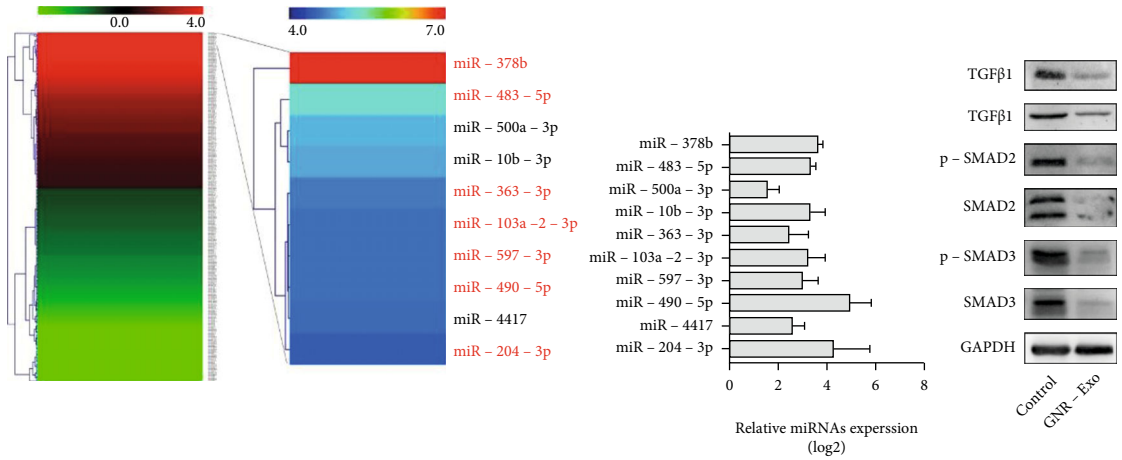

Figure 7: Possible mechanism of antitumor effect of GNRs-Exo. (a) Heatmap of hierarchical clustering of changed miRNAs. Values represent the log2 fold change of miRNAs for GNRs-Exo compared with the control exosomes. Green and red colors indicate downregulation and upregulation, respectively. (b) Heatmap of hierarchical clustering of interested miRNAs. (c) The expression of interested miRNAs was confirmed using RT-PCR. (d) GNRs–Exo disrupt the TGFβ pathway. GNRs–Exo inhibits the expression of TGFβ1, TGFβ2, SMAD2, and SMAD3 and was able to inactivate the phosphorylation of SMAD2 and SMAD3.

the possible mechanism of GNRs-Exo inhibiting tumor growth, we investigated the alterations of miRNAs in exosomes. Here, we isolated the exosomes from normal HRECs and GNR-treated binucleated HRECs. Then, we extracted total exosomal RNA and sent the samples to the Beijing Genomics Institute for miRNA gene sequencing. The data contained novel unknown miRNAs and known miRNAs, and we mainly focused on the known ones. There were 318 changed miRNAs in total, including 141 upregulated and 176 downregulated miRNAs (2-fold change) (Figure 7 (a)). We then verified the expression of top 10 annotated miRNAs using quantitative PCR (primers are shown in Table S1, and the Ct values are shown in Table S2) and found that the expression of these miRNAs in the GNR-Exo group was higher than that in the control exosome group (Figures 7(b) and 7(c)). Seven of the 10 miRNAs were reported to play antitumor roles which were marked in red [29–34]. Kyoto Encyclopedia of Genes and Genomes (KEGG) pathway analysis showed that the TGFβ pathway was downregulated in the GNR-Exo group (Fig. S3). Meanwhile, miR-483-5p, miR-363, miR-490-5p, and miR-204 were reported to regulate the transforming growth factor beta (TGFβ) signaling pathway [35–38].

The TGFβ signaling pathway involves multiple proteins such as TGFβ1, TGFβ2, SMAD1, SMAD2, and SMAD3 and the phosphorylated form of SMADs [39]. This signaling pathway played critical roles in cell growth, migration, invasion, differentiation, and extracellular matrix remodeling [39]. To clarify the possible molecular mechanism, we further examined the effect of GNRs-Exo on the TGFβ pathway. The results indicated that GNRs-Exo could inhibit the expression of TGFβ1, TGFβ2, SMAD2, and SMAD3 and was able to inactivate the phosphorylation of SMAD2 and SMAD3 (Figure 7(d)). All the data suggested that GNR-treated binucleated HRECs could secrete exosomes with altered content of miRNAs, and these miRNAs could suppress the TGFβ pathway to inhibit tumor growth *in vivo* and *in vitro*.

4. Conclusions

In summary, we engineered exosomes through changing the states and functions of vascular endothelial cells with PSS-GNRs. PSS-GNRs could induce the formation of binucleated HRECs and PSS-GNRs located in the endosomes. These two factors changed the exosomal miRNA profiles while they had no effect on the shape and size of exosomes. The engineered exosomes were able to suppress tumor growth in vitro and in vivo via disrupting the TGFβ pathway. These findings suggested that exosomes derived from PSS-GNR-treated binucleated ECs could be a promising biocompatible reagent for tumor therapy. Furthermore, this work also highlighted the potential of engineering exosomes inside mother cells using nanomaterials.

Data Availability

All data used to support the findings of this study are included within the article.

Conflicts of Interest

There are no conflicts to declare.

Authors' Contributions

Hongyuan Song and Wei Shen conceived and designed the project. Weiye Zhu, Zichang Zhao, Xiao Gui, Jiawei Zhao, Xiao Cui, Haorui Zhang, and Jianhua Zhang contributed in analysing and summarizing the data. Weiye Zhu, Na Zhao, Yukun Zhou, Rui Zhang, Ni Shen, Yanjie Li, Guangping Gao, and Haorui Zhang performed the experiment. Jianhua Zhang and Wei Shen drafted and revised the manuscript. Weiye Zhu, Rui Zhang, and Zichang Zhao contributed equally to this work.

Acknowledgments

This research was supported by the National Natural Science Foundation of China (82171081, 81800624, and 81700839), Shanghai Pujiang Program (21PD068), China Postdoctoral Science Foundation (2018M632122), "ChenGuang" project supported by the Shanghai Municipal Education Commission and the Shanghai Education Development Foundation (18CG40), and training program of basic medical foundation of Changhai Hospital (JC202117).

Supplementary Materials

FT-IR spectrum of gold nanorods, cell viability of PSS-GNR-treated HRECs, the changes of TGF-beta signaling pathway in gene sequencing data, primers used for miRNA quantification, and Ct value for miRNA quantification are included in the supplementary materials. *(Supplementary Materials)*

References

[1] H. Sung, J. Ferlay, R. L. Siegel et al., "Global cancer statistics 2020: GLOBOCAN estimatesof incidenceandmortalityworldwidefor36cancersin185countries," *CA: a Cancer Journal for Clinicians*, vol. 71, pp. 209–249, 2021.

[2] K. D. Miller, R. L. Siegel, C. C. Lin et al., "Cancer treatmentand survivorship statistics, 2016," *CA: acancerjournalforclinicians*, vol. 66, pp. 271–289, 2016.

[3] R. van der Meel, E. Sulheim, Y. Shi, F. Kiessling, W. J. Mulder, and T. Lammers, "Smart cancer nanomedicine," *Nature*, vol. 14, pp. 1007–1017, 2019.

[4] S. R. D'Mello, C. N. Cruz, M.-L. Chen, M. Kapoor, S. L. Lee, and K. M. Tyner, "The Evolving Landscapeofdrugproducts-containingnanomaterialsintheUnitedStates," *Naturenanotechnology*, vol. 12, pp. 523–529, 2017.

[5] S. Zanganeh, G. Hutter, R. Spitler et al., "Iron oxide nanoparticles inhibit tumour growth by inducing pro-inflammatory macrophage polarization in tumour tissues," *Nature Nanotechnology*, vol. 11, no. 11, pp. 986–994, 2016.

[6] S. Liu, X. Chen, L. Bao et al., "Treatment of infarcted heart tissue via the capture and local delivery of circulating exosomes through antibody-conjugated magnetic nanoparticles," vol. 4, no. 11, pp. 1063–1075, 2020.

[7] H. Y. Kim, T. J. Kim, L. Kang et al., "Mesenchymal stem cell-derived magnetic extracellular nanovesicles for targeting and treatment of ischemic stroke," *Biomaterials*, vol. 243, article 119942, 2020.

[8] D. M. Pegtel and S. J. Gould, "Exosomes," *Annual Review of Biochemistry*, vol. 88, no. 1, pp. 487–514, 2019.

[9] J. Kowal, M. Tkach, and C. Théry, "Biogenesis and secretionof exosomes," *Current Opinion in Cell Biology*, vol. 29, pp. 116–125, 2014.

[10] R. Kalluri, "The Biology and Function of Exosomesin Cancer," *The Journal of Clinical Investigation*, vol. 126, pp. 1208–1215, 2016.

[11] F. Pi, D. W. Binzel, T. J. Lee et al., "Nanoparticle orientation to control RNA loading and ligand display on extracellular vesicles for cancer regression," *Nature Nanotechnology*, vol. 13, pp. 82–89, 2018.

[12] M. Zhu, X. Tian, X. Song et al., "Nanoparticle-induced exosomes target antigen-presenting cells to initiate Th1-type immune activation," *Small*, vol. 8, no. 18, pp. 2841–2848, 2012.

[13] M. Zhu, Y. Li, J. Shi, W. Feng, G. Nie, and Y. Zhao, "Exosomes as extrapulmonary signaling conveyors for nanoparticle-induced systemic immune activation," *Small*, vol. 8, pp. 404–412, 2012.

[14] A. H. Alhasan, P. C. Patel, C. H. J. Choi, and C. A. Mirkin, "Exosome encased spherical nucleic acid gold nanoparticle conjugates as potent microRNA regulation agents," *Small*, vol. 10, pp. 186–192, 2014.

[15] V. Marchesano, Y. Hernandez, W. Salvenmoser et al., "Imaging inward and outward trafficking of gold nanoparticles in whole animals," *ACS Nano*, vol. 7, no. 3, pp. 2431–2442, 2013.

[16] H. Song, Q. Xu, H. Di, T. Guo, Z. Qi, and S. Zhao, "Time evolution and dynamic cellular uptake of PEGYlated gold nanorods," *RSC Advances*, vol. 6, pp. 8089–8092, 2016.

[17] C. Carnovale, G. Bryant, R. Shukla, and V. Bansal, "Identifying trends in gold nanoparticle toxicity and uptake: size, shape, capping ligand, and biological corona," *ACS Omega*, vol. 4, no. 1, pp. 242–256, 2019.

[18] W. S. Cho, M. Cho, J. Jeong et al., "Acute toxicity and pharmacokinetics of 13 nm-sized PEG-coated gold nanoparticles," *Toxicology and Applied Pharmacology*, vol. 236, no. 1, pp. 16–24, 2009.

[19] Z. Liu, L. Wang, L. Zhang et al., "Metabolic characteristics of 16HBE and A549 cells exposed to different surface modified gold nanorods," *Advanced Healthcare Materials*, vol. 5, no. 18, pp. 2363–2375, 2016.

[20] H. Song, T. Guo, Z. Zhao et al., "Biocompatible PEGylated gold nanorods function as cytokinesis inhibitors to suppress angiogenesis," *Biomaterials*, vol. 178, pp. 23–35, 2018.

[21] A. N. Paradis, M. S. Gay, and L. Zhang, "Binucleation of cardiomyocytes: the transition from a proliferative to a terminally differentiated state," *Drug Discovery Today*, vol. 19, no. 5, pp. 602–609, 2014.

[22] T. Zhou, M. Yu, B. Zhang et al., "Inhibitionof cancer cellmigrationby gold nanorods: molecular mechanismsand implicationsfor cancer therapy," *Advanced Functional Materials*, vol. 24, pp. 6922–6932, 2014.

[23] L. Wang, Y. Liu, W. Li et al., "Selective targetingof goldnanorodsatthemitochondriaofcancercells: implicationsfor cancer therapy," *Nano Letters*, vol. 11, pp. 772–780, 2011.

[24] C. Villarroya-Beltri, F. Baixauli, M. Mittelbrunn et al., "ISGylation controls exosome secretion by promoting lysosomal degradation of MVB proteins," *Nature Communications*, vol. 7, pp. 1–11, 2016.

[25] N. Ludwig, S. S. Yerneni, B. M. Razzo, and T. L. Whiteside, "Exosomes from HNSCC promote angiogenesis through reprogramming of endothelial cells," *Molecular Cancer Research*, vol. 16, no. 11, pp. 1798–1808, 2018.

[26] I. Li and B. Y. Nabet, "Exosomes in the tumor microenvironment as mediators of cancer therapy resistance," *Molecular Cancer*, vol. 18, no. 1, pp. 1–10, 2019.

[27] D. Hanahan, "Hallmarks of cancer: new dimensions," *Cancer Discovery*, vol. 12, no. 1, pp. 31–46, 2022.

[28] R. W. Carthew and E. J. Sontheimer, "Origins and mechanisms of miRNAs and siRNAs," *Cell*, vol. 136, pp. 642–655, 2009.

[29] G.-J. Zhang, H. Zhou, H.-X. Xiao, Y. Li, and T. Zhou, "MiR-378 is an independent prognostic factor and inhibits cell

growth and invasion in colorectal cancer," *BMC Cancer*, vol. 14, pp. 1–9, 2014.

[30] L. Wang, M. Shi, S. Hou et al., "MiR-483–5p suppresses the proliferation of glioma cells via directly targeting ERK1," *FEBS Letters*, vol. 586, pp. 1312–1317, 2012.

[31] F. Hu, J. Min, X. Cao et al., "MiR-363-3p inhibits the epithelial-to-mesenchymal transition and suppresses metastasis in colorectal cancer by targeting Sox4," *Biochemical and Biophysical Research Communications*, vol. 474, no. 1, pp. 35–42, 2016.

[32] J. Liang, X. Liu, H. Xue, B. Qiu, B. Wei, and K. Sun, "MicroRNA-103a inhibits gastric cancer cell proliferation, migration and invasion by targeting c-Myb," *Cell Proliferation*, vol. 48, pp. 78–85, 2015.

[33] J. He, J. Mai, Y. Li et al., "MiR-597 inhibits breast cancer cell proliferation, migrationand invasionthrough Fosl2," *Oncology Reports*, vol. 37, pp. 2672–2678, 2017.

[34] Z.-H. Cui, S.-Q. Shen, Z.-B. Chen, and C. Hu, "Growth inhibition of hepatocellular carcinoma tumor endothelial cells by miR-204-3p and underlying mechanism," *World Journalof Gastroenterology: WJG*, vol. 20, p. 5493, 2014.

[35] B. Xu, T. Xu, H. Liu, Q. Min, S. Wang, and Q. Song, "MiR-490-5p suppresses cell proliferation and invasion by targeting BUB1 in hepatocellular carcinoma cells," *Pharmacology*, vol. 100, no. 5-6, pp. 269–282, 2017.

[36] R. Xu, J. Li, B. Wei, W. Huo, and L. Wang, "MicroRNA-483-5p modulates the expression of cartilage-related genes in human chondrocytes through down-regulating TGF-β1 expression," *The Tohoku Journal of Experimental Medicine*, vol. 243, pp. 41–48, 2017.

[37] Y. Wang, W. Li, X. Zang et al., "MicroRNA-204-5p regulates epithelial-to-mesenchymal transition during human posterior capsule opacification by targeting Smad4," *Investigative Ophthalmology & Visual Science*, vol. 54, no. 1, pp. 323–332, 2013.

[38] F. Pan, H. Xiang, J. Yan et al., "Dendritic Cells from Rheumatoid Arthritis Patient Peripheral Blood Induce Th17 Cell Differentiation via miR-363/Integrin αv/TGF-β Axis," *Scandinavian Journal of Immunology*, vol. 85, pp. 441–449, 2017.

[39] E. H. Budi, D. Duan, and R. Derynck, "Transforming growth factor-β receptors and Smads: regulatory complexity and functional versatility," *Trends in Cell Biology*, vol. 27, no. 9, pp. 658–672, 2017.